AGU PUBLICATIONS

Geophysical Research Letters

RESEARCH LETTER

10.1002/2016GL071333

Key Points:
- Future increases in ocean heat transport to the Arctic are linked to reduced heat loss from the subpolar oceans
- Models with larger ocean heat transport increase to the Arctic Ocean exhibit greater Arctic amplification
- Greenhouse forced changes in ocean heat transport may not be coherent from middle to high latitudes

Supporting Information:
- Text S1
- Table S1

Correspondence to:
A. Nummelin,
aleksi.nummelin@uib.no

Citation:
Nummelin, A., C. Li, and P. J. Hezel (2017), Connecting ocean heat transport changes from the mid-latitudes to the Arctic Ocean, *Geophys. Res. Lett.*, *44*, 1899–1908, doi:10.1002/2016GL071333.

Received 24 SEP 2016
Accepted 27 JAN 2017
Accepted article online 31 JAN 2017
Published online 17 FEB 2017

Connecting ocean heat transport changes from the midlatitudes to the Arctic Ocean

Aleksi Nummelin[1,2], Camille Li[1,2], and Paul J. Hezel[1,2]

[1]Geophysical Institute, University of Bergen, Bergen, Norway, [2]Bjerknes Centre for Climate Research, Bergen, Norway

Abstract Under greenhouse warming, climate models simulate a weakening of the Atlantic Meridional Overturning Circulation and the associated ocean heat transport at midlatitudes but an increase in the ocean heat transport to the Arctic Ocean. These opposing trends lead to what could appear to be a discrepancy in the reported ocean contribution to Arctic amplification. This study clarifies how ocean heat transport affects Arctic climate under strong greenhouse warming using a set of the 21st century simulations performed within the Coupled Model Intercomparison Project. The results suggest that a future reduction in subpolar ocean heat loss enhances ocean heat transport to the Arctic Ocean, driving an increase in Arctic Ocean heat content and contributing to the intermodel spread in Arctic amplification. The results caution against extrapolating the forced oceanic signal from the midlatitudes to the Arctic.

1. Introduction

The ocean and atmosphere transport heat from areas of net heat gain in the tropics to areas of net heat loss at high latitudes. Under global warming, atmospheric heat transport is expected to increase, mostly because warmer air can hold more water vapor, thus enhancing the latent heat transport [*Manabe and Stouffer*, 1980; *Held and Soden*, 2006]. A warmer and wetter atmosphere reduces the potential for heat loss from the ocean and enhances freshwater input at high latitudes via increased precipitation, runoff, and melting ice [*Haine et al.*, 2015]. In the North Atlantic, the result is that convecting water masses become less dense, ultimately weakening the Atlantic Meridional Overturning Circulation (AMOC) [*Collins et al.*, 2013].

Ocean circulation changes help shape the response to greenhouse warming in the North Atlantic [*Marshall et al.*, 2014, 2015; *Winton et al.*, 2013]. The weakened AMOC reduces ocean heat transport in the midlatitudes, leading to the well-documented "warming hole," a region of relatively weak ocean warming visible in models and observations [*Drijfhout et al.*, 2012; *Collins et al.*, 2013; *Rahmstorf et al.*, 2015]. In the Arctic, changes in ocean circulation are small while ocean temperatures and heat transport both increase [*Spielhagen et al.*, 2011; *Koenigk and Brodeau*, 2014]. It would therefore appear that changes in northern high-latitude ocean heat transport are somewhat disconnected from their lower latitude counterparts.

This apparent disconnect also has implications for our understanding of Arctic amplification (AA), whereby the Arctic warms faster than the rest of the globe. Attempts to connect AA to ocean changes yield differing answers. Studies focusing on ocean regions where the AMOC response dominates find that changes in ocean heat transport are not related to, or indeed weakly oppose, AA [*Rugenstein et al.*, 2013; *Pithan and Mauritsen*, 2014]. Conversely, studies focusing on high-latitude oceans conclude that ocean heat transport contributes to AA [*Holland and Bitz*, 2003; *Mahlstein and Knutti*, 2011; *Hodson et al.*, 2013; *Hwang et al.*, 2011]. These differences raise questions about the exact link between the AMOC, ocean heat transport, and high-latitude climate change.

The subpolar region is likely critical to understanding this link. Previous studies point separately to its roles in weakening the AMOC [*Brodeau and Koenigk*, 2016; *Gregory et al.*, 2005] and strengthening ocean heat transport [*Koenigk and Brodeau*, 2014; *Marshall et al.*, 2015] under global warming. The overall response of the ocean heat content at any given location arises from a competition between changing ocean heat transport and changing surface heat fluxes, the outcome of which can depend on the model and forcing scenario. Furthermore, it is not just the local competition that matters, since surface heat fluxes south of a given location partly determine ocean heat transport to that location. To arrive at a consistent picture of the Arctic-Atlantic response to greenhouse forcing, we must thus consider both the atmosphere-ocean coupling and the meridional connections via the subpolar ocean.

Table 1. List of Symbols

Symbol	Name	Unit
A	Grid cell area	m^2
c_p	Specific heat capacity of sea water	J kg^{-1} K^{-1}
Δt	95 year time period from 2005 to 2100	s
$\overline{H_L}$	Mean latent heat flux trend at the base of the atmosphere (positive down)	W m^{-2}
$\overline{H_S}$	Mean sensible heat flux trend at the base of the atmosphere (positive down)	W m^{-2}
HTC	Ocean heat transport convergence	W m^{-2}
$\overline{\text{HTC}}$	Mean ocean heat transport convergence trend	W m^{-2}
$\overline{\text{IHC}'}$	Mean sea ice heat content trend	W m^{-2}
k_{HTC}	Regression slope of the ocean heat transport convergence	W m^{-2} s^{-1}
$k_{\text{OHC}'}$	Regression slope of the ocean heat content tendency	W m^{-2} s^{-1}
k_{SFL}	Regression slope of the surface heat flux	W m^{-2} s^{-1}
OHC	Ocean heat content	J m^{-2}
OHC'	Ocean heat content tendency	W m^{-2}
$\overline{\text{OHC}'}$	Mean ocean heat content tendency trend	W m^{-2}
ρ	Density of sea water	kg m^{-3}
$\overline{R_{\text{LWnet}}}$	Mean longwave radiation trend at the base of the atmosphere (positive down)	W m^{-2}
$\overline{R_{\text{SWnet}}}$	Mean shortwave radiation trend at the base of the atmosphere (positive down)	W m^{-2}
SFL	Surface heat flux at the ocean surface (positive down)	W m^{-2}
$\overline{\text{SFL}}$	Mean surface heat flux trend at the ocean surface (positive down)	W m^{-2}
SFLa	Surface heat flux at the base of the atmosphere (positive down)	W m^{-2}
$\overline{\text{SFLa}}$	Mean surface heat flux trend at the base of the atmosphere (positive down)	W m^{-2}
T	Temperature of sea water	K
t	Time	s
z	Ocean depth	m

Here we aim to clarify the role of ocean heat transport in Arctic climate change within the context of broader changes in the Northern Hemisphere. We examine how ocean heat transport is linked to ocean heat content and atmospheric temperature trends in a set of future climate change projections under the Coupled Model Intercomparison Project (CMIP5) and use this framework to resolve apparent contradictions in the literature. Our results suggest that under greenhouse forcing, reduced heat loss from the subpolar ocean can increase ocean heat transport to the Arctic regardless of the AMOC response. The strength of the subpolar response is model dependent and ultimately contributes to the intermodel spread in Arctic amplification.

2. Methods

This study uses heat budget trends in a subset of 20 CMIP5 model simulations (Table S1 in the supporting information) under the RCP8.5 scenario for the period 2005–2100.

We start with the vertically integrated ocean heat budget as follows:

$$\text{OHC}'(t) = \text{SFL}(t) + \text{HTC}(t) \tag{1}$$

where t is time, $\text{OHC}'(t)$ is the ocean heat content tendency, $\text{SFL}(t)$ is the surface heat flux (positive into the ocean), and $\text{HTC}(t)$ is the ocean heat transport convergence (see Table 1 for list of variables used). We approximate changes in the heat budget under RCP8.5 as a linear process of the form $\text{OHC}'(t) \approx k_{\text{OHC}'}t$, $\text{SFL}(t) \approx k_{\text{SFL}}t$, and $\text{HTC}(t) \approx k_{\text{HTC}}t$, where k is the slope of the linear least squares fit to the model data. Integrating over the 95 year (2005–2100) simulation period (Δt) and dividing by Δt gives

$$\int_0^{\Delta t} k'_{\text{OHC}} t\,dt \approx \int_0^{\Delta t} (k_{\text{SFL}}t + k_{\text{HTC}}t)dt \tag{2}$$

$$\overbrace{\frac{\Delta t}{2}k_{\text{OHC}'}}^{\overline{\text{OHC}'}} \approx \overbrace{\frac{\Delta t}{2}k_{\text{SFL}}}^{\overline{\text{SFL}}} + \overbrace{\frac{\Delta t}{2}k_{\text{HTC}}}^{\overline{\text{HTC}}} \tag{3}$$

Rather than using the flux trends k [W m^{-2} s^{-1}], we use the time-integrated quantities $\overline{\mathrm{OHC}'}$, $\overline{\mathrm{SFL}}$, and $\overline{\mathrm{HTC}}$, [W m^{-2}] for each trend, which allows for a direct comparison with other radiative and flux terms. We refer to these time-integrated quantities as trends for simplicity. Because the strong RCP8.5 forcing dominates the model trajectories, we do not remove any possible preindustrial control simulation drift before calculating the trends.

We analyze zonal averages or sums over the ocean. These calculations are straightforward for the atmospheric output, which is on a latitude-longitude grid. The ocean output is on different grids, so we simply take the zonal average/sum over all grid cells within a ±0.5° latitude band around each latitude value. When the grid is coarser than 1°, the missing bands are filled with linear interpolation. SFL is the net surface heat flux (sum of longwave, shortwave, sensible, and latent heat) at the ocean surface and a direct ocean model output. We calculate HTC from the monthly mean zonally integrated northward ocean heat transport output (hfbasin in CMIP5). We calculate the vertically integrated OHC using

$$\mathrm{OHC}(t) = \sum_{z=z_1}^{Z} c_p T(z,t)\rho(z,t)A\Delta z \tag{4}$$

where $c_p = 4000$ J kg^{-1} K^{-1} is a constant heat capacity, $T(z,t)$ is temperature, $\rho(z,t)$ is density, A is the grid cell area, and Δz is the thickness of a given layer z. The density ρ is calculated using the EOS-80 standard for equation of state of seawater. The errors arising from this offline OHC calculation are small for our purposes, especially because we are interested in trends rather than absolute values. We approximate the OHC tendency (OHC′) using annual means. Even with this simplified approach, the results are robust as the derivative of a quadratic fit to the OHC data yields a trend value almost identical to $k_{\mathrm{OHC}'}$.

Flux trends are defined as positive when they increase ocean heat content. The physical interpretation is straightforward for OHC′ and HTC. For SFL in middle to high latitudes, the annual mean surface heat flux acts to cool the ocean (negative), so a positive trend indicates reduced cooling, i.e., ocean warming by retention of heat. This sign convection holds for the longwave, sensible, and latent heat flux components of SFL; the shortwave component always acts to warm the ocean, so a positive trend actually means increased warming.

For the Norwegian Earth System Model (NorESM1-M) we have all the terms in equation (3), but our analysis of the CMIP5 multimodel ensemble is restricted by the lack of comprehensive ocean model output. For the full ensemble, we have only two relevant variables: OHC′ and SFLa. SFLa is the net surface heat flux at the base of the atmosphere and can differ from SFL, the net surface flux at the ocean surface, when sea ice is present due to latent heat processes. We can write the heat budget at the base of the atmosphere as

$$\overline{\mathrm{OHC}'} \approx \overline{\mathrm{SFLa}} + (\overline{\mathrm{HTC}} - \overline{\mathrm{IHC}'}) \tag{5}$$

where $\overline{\mathrm{IHC}'}$ is the contribution from the sea ice heat content trend. In this framework the difference between $\overline{\mathrm{OHC}'}$ and $\overline{\mathrm{SFLa}}$ is the ocean heat transport convergence including changes in sea ice cover.

3. Results and Discussion

3.1. Heat Budget Trends in the Norwegian Earth System Model

Under CO_2-driven warming, the global ocean acts as a heat sink. The rate of heat uptake varies geographically (Figure 1a) with a pattern comparable to observed upper ocean heat content and temperature trends [*Levitus et al.*, 2012; *Wu et al.*, 2012]. Here we focus on three regions in the extratropical Northern Hemisphere: the midlatitude oceans (region A, 30°N–50°N) and Arctic Ocean (region C, north of 77°N), both of which exhibit strong positive OHC′ trends, and the subpolar oceans (region B, 50°N–77°N) which exhibit weaker positive OHC′ trends (Figure 1b).

In region A, the OHC′ trend (Figure 1b, gray) is driven by two factors related to the poleward expansion of the Hadley cell, a well-documented response to greenhouse warming [*Fu et al.*, 2006; *Johanson and Fu*, 2009; *Tandon et al.*, 2013; *Hu et al.*, 2013; *Tao et al.*, 2016; *Collins et al.*, 2013]. First, a poleward expansion of the subtropical high-pressure regions [*Lu et al.*, 2007; *Hu et al.*, 2013] produces positive surface heat flux trends over region A (Figure 1b, orange; see details in section 3.2). Second, a poleward migration of the surface wind stress curl pattern (Figure S2) produces a poleward shift of the ocean heat transport convergence around 43°N

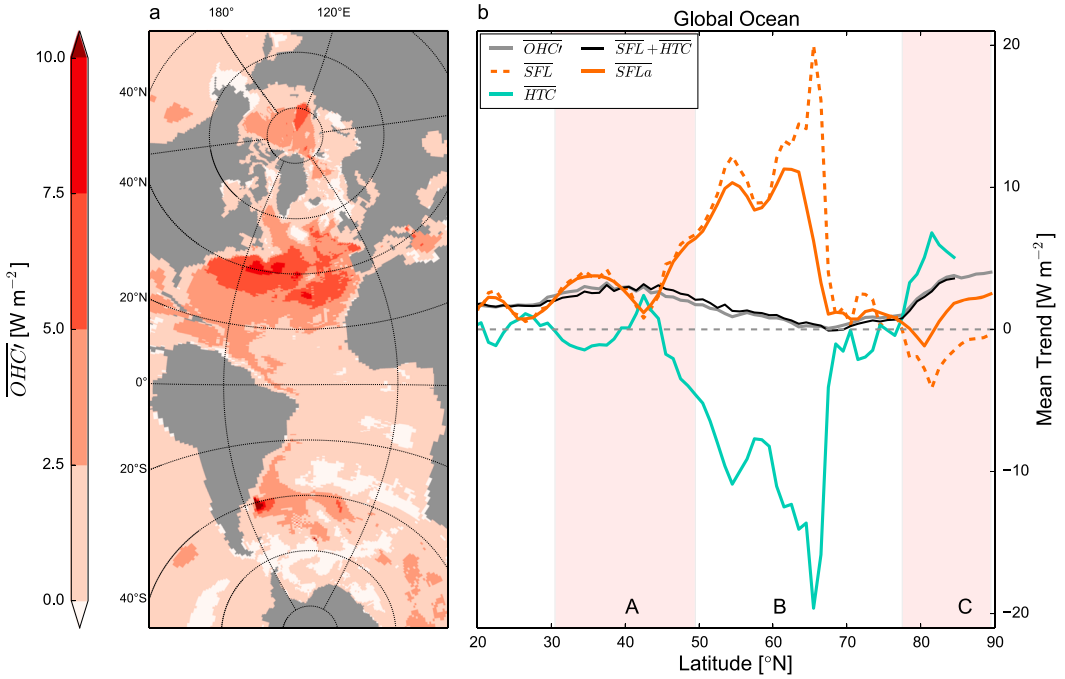

Figure 1. Vertically integrated ocean heat budget terms (equation (3)) in the Norwegian Earth System Model (NorESM1-M) under the RCP8.5 scenario (2005–2100). (a) Heat content tendency trend $\overline{OHC'}$ (W m^{-2}) in the Arctic-Atlantic sector. (b) Zonal mean trends in ocean heat content tendency $\overline{OHC'}$ (W m^{-2}); surface heat flux at the ocean surface $\overline{SFL}$ (W m^{-2}); ocean heat transport convergence $\overline{HTC}$ (W m^{-2}); the sum of $\overline{SFL}$ and $\overline{HTC}$, which should be equal to $\overline{OHC'}$ if linear assumption holds; and surface heat flux at the base of the atmosphere $\overline{SFLa}$ (W m^{-2}). Regions A, B, and C are the midlatitude, subpolar, and Arctic latitude bands.

(Figure 1b, green, similar to *Saenko et al.* [2005]). The positive $\overline{OHC'}$ in region A is similar in structure to sea surface temperature trends in the historical period deduced from observations and models [*Wu et al.*, 2012; *Yang et al.*, 2016].

In region B, the OHC′ trends are small because there is a rough balance between the reduced ocean heat transport convergence (Figure 1b, green) and reduced surface heat loss to the atmosphere (i.e., positive $\overline{SFLa}$, Figure 1b, solid orange). As the atmosphere warms faster than the surface ocean in RCP8.5, the weakening temperature contrast leads to reduced turbulent heat fluxes from the ocean to the atmosphere (similar to *Brodeau and Koenigk* [2016]; see details in section 3.2). The reduced ocean heat loss, enhanced freshwater input, and northward shift and weakening of the wind stress curl pattern lead to weaker overturning (Figure S3) [*Collins et al.*, 2013; *Brodeau and Koenigk*, 2016] and a weaker subpolar gyre circulation (Figure S4) (similar to *Yang and Saenko* [2012] and *Reintges et al.* [2016]). The result is a negative trend in ocean heat transport convergence in region B. In addition, as the Arctic sea ice cover diminishes, less sea ice is exported to region B. Therefore, less of the ocean heat is used to melt ice, resulting in a larger positive heat flux trend at the ocean surface ($\overline{SFL}$, dashed orange) than at the base of the atmosphere ($\overline{SFLa}$, orange).

Farther north in region C, ocean heat transport convergence increases and drives a positive OHC′ trend (Figure 1b). The ocean loses more heat (negative $\overline{SFL}$, dashed orange), but the amount delivered to the base of the atmosphere ($\overline{SFLa}$, orange) is additionally affected by sea ice changes and an increasing proportion of rain to snowfall. Winter sea ice retreat near 80°N allows the atmosphere to receive more heat and produces the $\overline{SFLa}$ minimum there. North of 80°N, the effects of summer ice retreat allow enhanced surface absorption of solar radiation, and $\overline{SFLa}$ becomes positive (see section 3.2).

3.2. Heat Budget Trends in the CMIP5 Ensemble

Next we expand the ocean heat budget analysis to the CMIP5 ensemble. Due to a lack of available model output, we base our analysis on equation (5)—that is, we infer the ocean heat transport convergence trends based on the difference between the ocean heat content tendency trend and the surface heat flux trend. To clarify the physical relationships, we decompose the surface heat flux trend into its constituent terms.

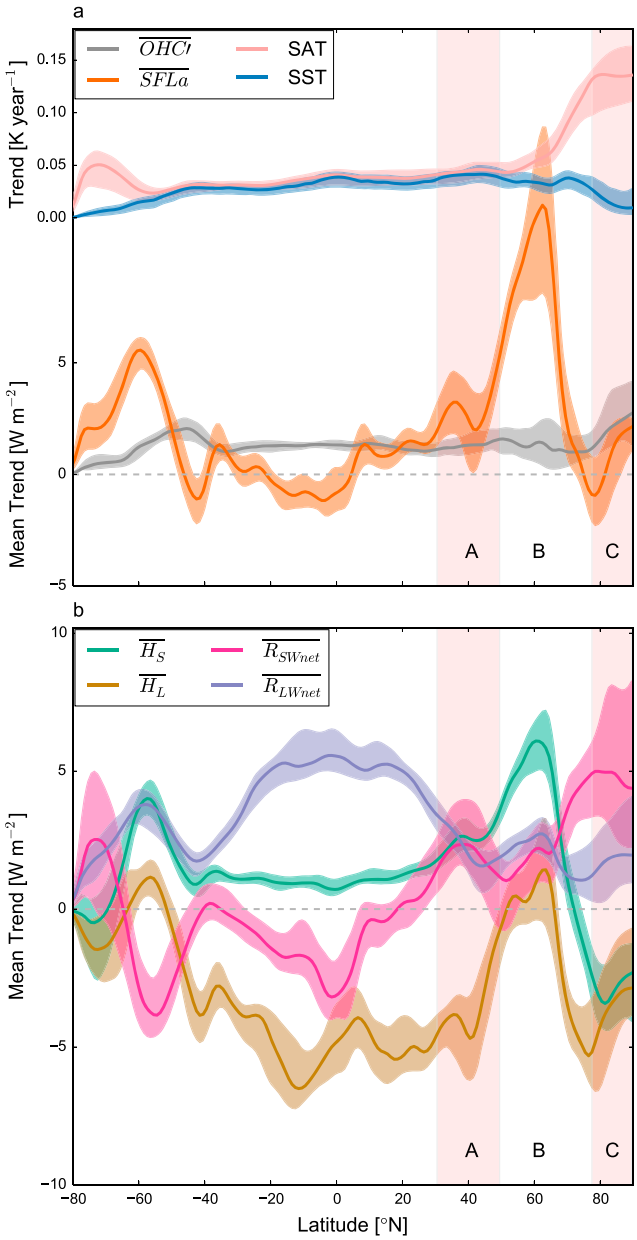

Figure 2. Vertically integrated ocean heat budget terms and surface heat fluxes in 20 CMIP5 models (Table S1) under the RCP8.5 scenario (2005–2100). (a) Zonal mean trends in ocean heat content tendency $\overline{OHC'}$ (W m^{-2}), surface heat flux at the base of the atmosphere $\overline{SFLa}$ (W m^{-2}), sea surface temperature SST (K yr^{-1}), and surface air temperature SAT (K yr^{-1}). (b) Breakdown of $\overline{SFLa}$ into its constituent terms (W m^{-2}): trends in sensible heat flux $\overline{H_s}$, latent heat flux $\overline{H_L}$, shortwave radiation $\overline{R_{SWnet}}$, and longwave radiation $\overline{R_{LWnet}}$. Solid lines are the multimodel medians, while shading shows the interquartile range (25%–75%). Regions A, B, and C are the midlatitude, subpolar, and Arctic latitude bands. Data are spatially smoothed with a 5° low-pass filter.

Generally, we find positive $\overline{OHC'}$ in the Arctic Ocean (region C) similar to NorESM1-M but weak $\overline{OHC'}$ in regions A and B (Figure 2a). The weaker apparent trends in regions A and B result from averaging over different meridional structures in $\overline{OHC'}$ in each CMIP5 model (Figure S1).

In region A, consistent with NorESM1-M results, the ocean response is due to the well-documented northward expansion of the Hadley cell. This causes a poleward expansion of the dry subtropical high-pressure regions and associated reduction in cloudiness, which results in a positive trend in the shortwave radiative flux (Figure 2b, red).

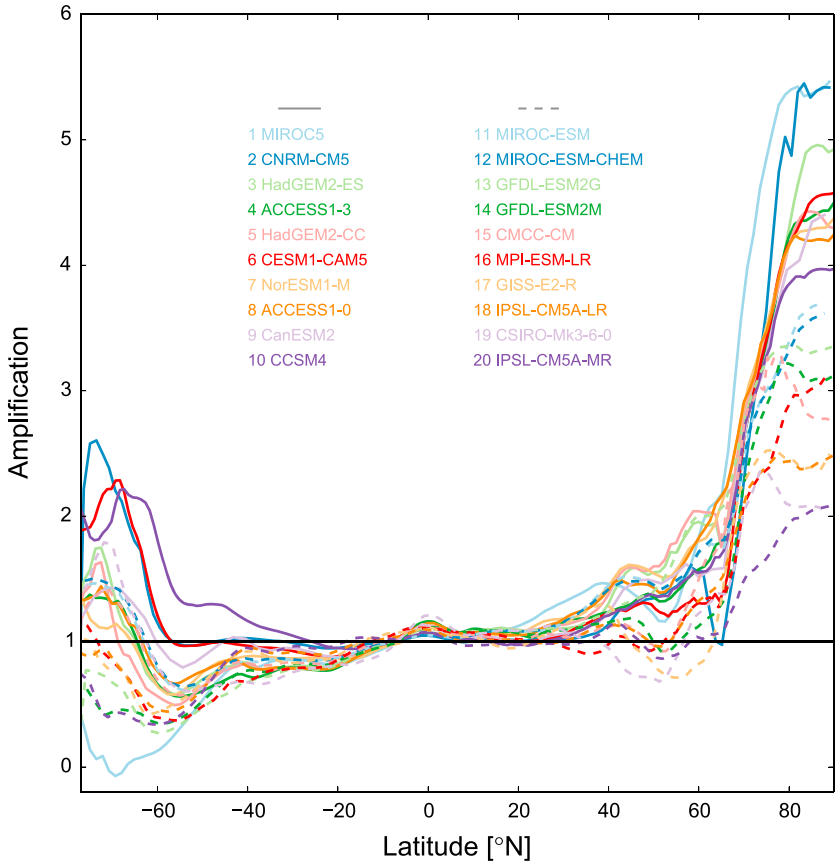

Figure 3. Amplification of greenhouse warming over the ocean by latitude in 20 CMIP5 models under the RCP8.5 scenario (2005–2100). Models are listed in order of Arctic amplification (area averaged over region C, i.e., north of 77°N), with amplification as defined in section 3.3.

In region B, the ocean heat content tendency trends are small despite the large positive surface heat flux trends, which leads us to infer a reduction in the ocean heat transport convergence trends similar to trends in NorESM1-M (Figure 2a). As in NorESM1-M, the surface heat loss weakens (positive $\overline{\mathrm{SFLa}}$) because the atmosphere warms faster than the surface ocean (Figure 2a, pink and blue). The warmer and moister atmosphere leads to reduced sensible and latent heat loss from the ocean (Figure 2b, green and gold show generally positive trends).

In region C, the ocean gains more heat than can be attributed to the reduced surface heat loss to the atmosphere (Figure 2a, compare gray and orange lines). This implies that ocean heat transport into the Arctic must increase. Similar to NorESM1-M, the CMIP5 ensemble mean surface heat flux trend is negative around 80°N (Figure 2a)–turbulent heat fluxes vent more heat from the ocean than the radiative fluxes provide (Figure 2b). Therefore, in this region, the increased ocean heat transport convergence must account for both the increased ocean heat content as well as the increased heat loss to the atmosphere.

The increased ocean heat transport to the Arctic could be due to either increasing ocean temperatures or volume transports, or a combination of both. Based on the overturning stream function response, increased volume transports seem to contribute more in some models [*Bitz et al.*, 2006; *Marshall et al.*, 2015], but analysis of two NorESM simulations (not shown) indicates that warmer ocean temperatures dominate the heat transport signal in this model (similar to *Koenigk and Brodeau* [2014]). We find no volume transport trends through the main Arctic straits despite a slightly stronger overturning circulation north of 80°N (the overturning stream function includes flow confined within the Arctic basin as well as actual inflows and outflows).

3.3. Ensemble Spread in Arctic Amplification

While all the CMIP5 models exhibit Arctic amplification (AA), there is considerable spread in the intensity of the amplification (Figure 3). We define the amplification of greenhouse warming as the ratio between local and

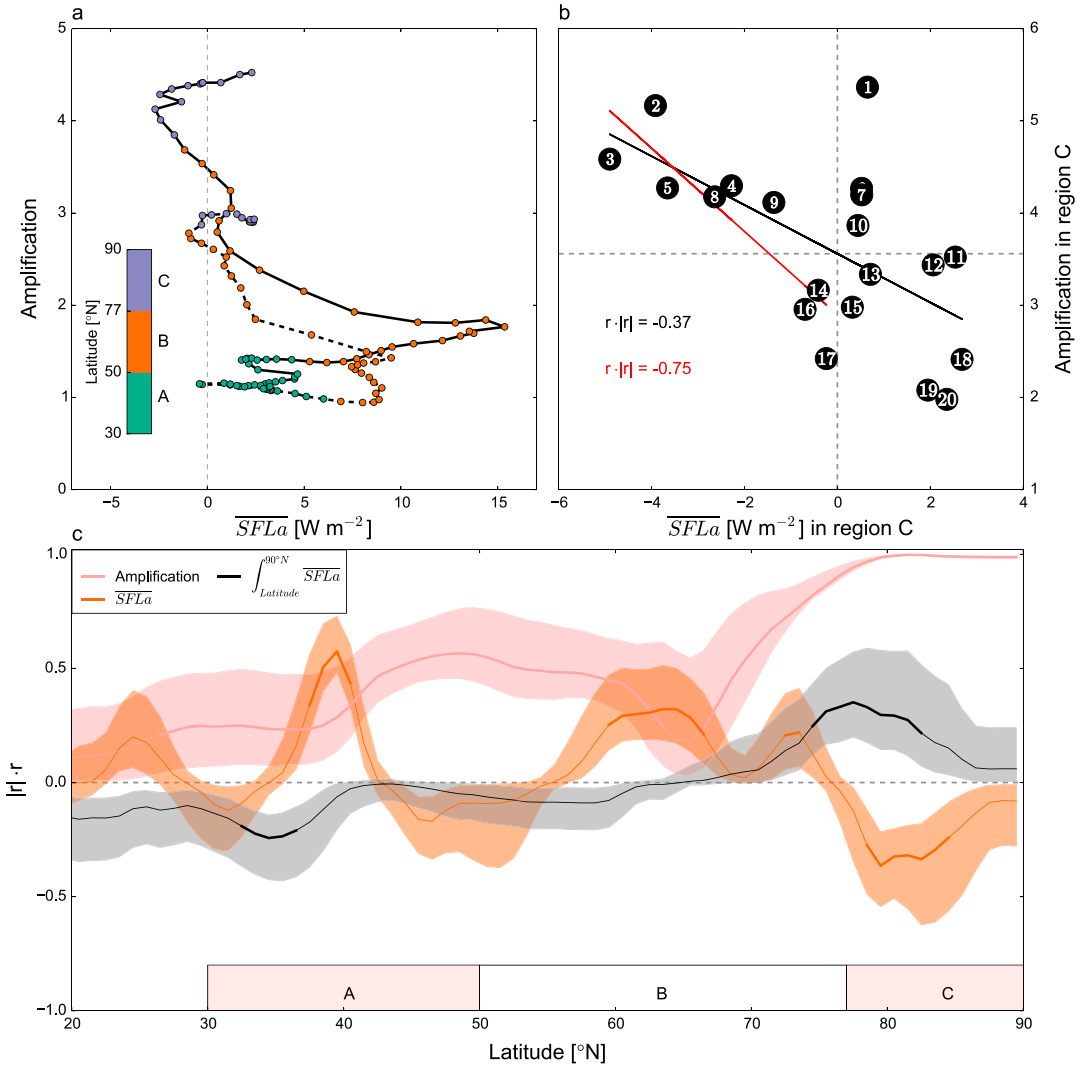

Figure 4. Intermodel spread of heat flux trends and Arctic amplification across 20 CMIP5 models (Table S1) under the RCP8.5 scenario (2005–2100). (a) Trend in surface heat flux $\overline{OHC'}$ (W m^{-2}) versus local amplification for the 10 models with the most Arctic amplification (solid line) and the 10 models with the least Arctic amplification (dashed line; see Figure 3 for the two model groups). The data are smoothed with a 5° running mean. (b) Scatterplot of Arctic amplification and Arctic (region C) heat flux trends, where negative trends indicate increased ocean heat loss. Numbers correspond to model numbers in Figure 3. The horizontal line separates the 10 models with the most Arctic amplification from the 10 models with the least Arctic amplification. The black fit is for all 20 models; the red fit is for the models with increased ocean heat loss in the Arctic. (c) Directional shared covariance $|r| \cdot r$ (i.e., Pearson correlation coefficient squared but retaining the sign of the correlation) between Arctic amplification and zonal mean local amplification, surface heat flux trend $\overline{\text{SFLa}}$ (W m^{-2}), and $\overline{\text{SFLa}}$ integrated north of each latitude (proxy for ocean heat transport). Thick lines indicate significance, i.e., regression slopes that are significantly different from zero at the 95% level using a two-sided student's *t* test. The shading illustrates robustness of the shared covariance to outliers via a Monte Carlo-based interquartile range (10000 samples of shared covariance using 10 randomly picked models). Regions A, B, and C are the midlatitude, subpolar, and Arctic latitude bands.

tropical (30°S–30°N) surface air temperature trends over the ocean and AA as the area-averaged amplification in region C. The Northern Hemisphere amplification begins to manifest at latitudes between 40°N and 60°N depending on the model, and the AA factor varies from 2 to over 5, which is comparable to previous model results [*Holland and Bitz*, 2003] and other definitions of the amplification factor [*Holland and Landrum*, 2015].

The CMIP5 model results suggest a consistent meridional relationship between AA and surface heat flux trends from midlatitudes to the Arctic. The ocean retains heat at subpolar latitudes and releases more heat to

the atmosphere farther to the north and more so for models that have stronger AA (Figure 4a, compare solid and dashed). AA is significantly correlated with Arctic surface heat loss across all models (Figure 4b; $r^2 = 0.37$), but the relationship is stronger for models in which Arctic surface heat loss increases (negative $\overline{\text{SFLa}}$; red in Figure 4b; $r^2 = 0.75$; see also text S2 and Figures S5–S7).

In fact, the intermodel spread in AA can be linked with the intermodel spread in ocean heat budget trends from the midlatitudes to the Arctic. Figure 4c shows the correlation across all the models (in terms of directional shared variance; see caption) between AA and local amplification, surface heat flux trend, and the surface heat flux trend north of each latitude, which can be considered to be the portion of the ocean heat transport that the atmosphere feels. Models with high AA have high amplification in the 40°N–60°N band (pink; approximately 50% shared variance). This relationship weakens around 60°N–70°N, where a stronger link to surface heat flux trends emerges: models with high AA tend to have the largest reductions in subpolar ocean heat loss (orange). North of 75°N, the relationship switches sign, with stronger AA linked to increased ocean heat loss (orange, also shown in Figure 4b) and increased ocean heat transport to the high latitudes (black).

Understanding these meridional dependencies helps to put results from previous studies [*Holland and Bitz*, 2003; *Hwang et al.*, 2011; *Mahlstein and Knutti*, 2011; *Pithan and Mauritsen*, 2014] in a common framework. By focusing on different latitudes, these studies effectively sample the curves in Figure 4c at different locations and thus identify different aspects of the answer. At 60°N, the intermodel spread in ocean heat transport and in AA is not linked (gray curve close to 0), consistent with *Pithan and Mauritsen* [2014]. When considering regions farther north, a positive relationship emerges whereby models with stronger ocean heat transport exhibit stronger AA (gray curve becomes positive), consistent with *Holland and Bitz* [2003], *Hwang et al.* [2011], and *Mahlstein and Knutti* [2011].

Finally, the results say that, across a large suite of CMIP5 models under strong greenhouse forcing, AA is generally associated with decreased ocean heat transport to the midlatitudes (due to buoyancy forced circulation changes) and enhanced ocean heat transport to the Arctic (due to warmer ocean temperatures). However, these relationships can be different across a smaller set of models or under weaker forcing. For example, across various versions of the Geophysical Fluid Dynamics Laboratory model, a weakening AMOC is associated with weaker ocean heat transport to high latitudes and less AA [*Rugenstein et al.*, 2013; *Winton et al.*, 2013, 2014; *Trossman et al.*, 2016]. It is perhaps to be expected that AMOC changes are important in explaining model spread in this case, when the models differ primarily in their ocean components.

4. Concluding Remarks

The rate of ocean heat content increase varies geographically in the CMIP5 models, with the Arctic and midlatitude oceans showing the largest trends. While increasing ocean heat content in the northern midlatitudes is linked to an expansion of the Hadley cell, in the Arctic Ocean it is linked to enhanced ocean heat transport. We find that ocean heat transport to the Arctic increases because reduced surface heat loss at subpolar latitudes leaves more heat in the ocean. This linkage between subpolar heat fluxes and Arctic Ocean heat content has a parallel in the Southern Ocean, where reduced ocean heat loss south of 50°S results in enhanced ocean heat transport by equatorward flowing surface waters and an increase in ocean heat content to the north [*Armour et al.*, 2016].

Our results confirm a role for the ocean in Arctic warming. The oceanic response to greenhouse warming contributes to AA, alongside more important feedbacks [*Pithan and Mauritsen*, 2014; *Laîné et al.*, 2016]. Our analyses also resolve the apparent disconnect between middle-latitude and high-latitude ocean heat transport changes in the Northern Hemisphere under global warming. The changes in both regions are in part due to reduced subpolar heat loss, which weakens ocean heat transport to the midlatitudes but ultimately enhances ocean heat transport to the Arctic. The relationships between surface heat fluxes, Arctic amplification, and ocean heat transport help explain why models with high Arctic amplification tend to have the strongest increases in ocean heat transport to the Arctic and the strongest decreases in ocean heat transport to the midlatitudes (Figure 4c). Our results also indicate that the intermodel spread in temperature amplification is coherent across a wide latitude band from the midlatitudes to the Arctic Ocean (Figure 4c). Therefore, a path toward more robust projections of Arctic amplification would be to identify model-to-model differences in mechanisms that influence amplification across this entire band.

The results of this paper are robust across a diverse set of models, but we acknowledge that the underlying simulations represent transient climates under strong greenhouse forcing. The relationships and mechanisms identified here can be different under different forcings [*Bitz et al.*, 2006; *Delworth and Zeng*, 2016], when the role of internal variability is stronger [*Jungclaus et al.*, 2014], when considering equilibrium climates [*Kay et al.*, 2012], when analyzing a limited set of closely related models [*Rugenstein et al.*, 2013; *Winton et al.*, 2013, 2014; *Trossman et al.*, 2016], or when different definitions of the Arctic are used [*Holland and Bitz*, 2003; *Hwang et al.*, 2011; *Mahlstein and Knutti*, 2011; *Pithan and Mauritsen*, 2014].

Finally, the interplay between greenhouse forcing and internal variability is likely important for interpreting observations as well as transient climate change simulations. Other studies have demonstrated that internal variability drives coherent ocean heat transport changes across the entire North Atlantic-Arctic sector [*Årthun and Eldevik*, 2016; *Zhang*, 2015; *Yeager et al.*, 2015; *Onarheim et al.*, 2015]. Our work shows that, under strong greenhouse forcing, the spatial pattern of ocean heat transport variability is one of opposing changes in the midlatitudes versus the Arctic Ocean. One implication is that forced changes in ocean heat transport to the Arctic Ocean will be difficult to assess using observations from measurement arrays that are located south of the subpolar region (e.g., RAPID, *McCarthy et al.* [2015], and the OSNAP project, http://www.o-snap.org/observations/].

Acknowledgments

We would like to thank M. Huber, I. Medhaug, L.H. Smedsrud, T. Toniazzo, L. Zanna, and two anonymous reviewers for helpful discussions and comments on this manuscript. We acknowledge the World Climate Research Programme's Working Group on Coupled Modelling for CMIP data, and we thank the climate modeling groups (listed in Table S1 of this paper) for producing and making available their model output (at https://pcmdi.llnl.gov/search/esgf-llnl/). For CMIP, the U.S. Department of Energy's Program for Climate Model Diagnosis and Intercomparison provides coordinating support and led development of software infrastructure in partnership with the Global Organization for Earth System Science Portals. Python analysis scripts are available by contacting aleksi.nummelin@uib.no. This work was supported by the Bjerknes Centre SKD project DYNAWARM and the Research Council of Norway project DynAMiTe (255027). Finally, we thank E. Farmer for her copyediting services.

References

Armour, K. C., J. Marshall, J. R. Scott, A. Donohoe, and E. R. Newsom (2016), Southern Ocean warming delayed by circumpolar upwelling and equatorward transport, *Nat. Geosci.*, *9*, 549–554, doi:10.1038/ngeo2731.

Årthun, M., and T. Eldevik (2016), On anomalous ocean heat transport toward the arctic and associated climate predictability, *J. Clim.*, *29*(2), 689–704, doi:10.1175/JCLI-D-15-0448.1.

Bitz, C., P. Gent, R. Woodgate, M. Holland, and R. Lindsay (2006), The influence of sea ice on ocean heat uptake in response to increasing CO2, *J. Clim.*, *19*(11), 2437–2450, doi:10.1175/JCLI3756.1.

Brodeau, L., and T. Koenigk (2016), Extinction of the northern oceanic deep convection in an ensemble of climate model simulations of the 20th and 21st centuries, *Clim. Dyn.*, *46*(9–10), 2863–2882, doi:10.1007/s00382-015-2736-5.

Collins, M., et al. (2013), Long-term climate change: Projections, commitments and irreversibility, in *Climate Change 2013: The Physical Science Basis. Contribution of Working Group I to the Fifth Assessment Report of the Intergovernmental Panel on Climate Change*, edited by T. Stocker et al., pp. 1029–1136, Cambridge Univ. Press, Cambridge, U. K., and New York, doi:10.1017/CBO9781107415324.024

Delworth, T. L., and F. Zeng (2016), The impact of the North Atlantic Oscillation on climate through its influence on the Atlantic Meridional overturning circulation, *J. Clim.*, *29*(3), 941–962, doi:10.1175/JCLI-D-15-0396.1.

Drijfhout, S., G. J. van Oldenborgh, and A. Cimatoribus (2012), Is a decline of AMOC causing the warming hole above the North Atlantic in observed and modeled warming patterns?, *J. Clim.*, *25*(24), 8373–8379, doi:10.1175/JCLI-D-12-00490.1.

Fu, Q., C. M. Johanson, J. M. Wallace, and T. Reichler (2006), Enhanced mid-latitude tropospheric warming in satellite measurements, *Science*, *312*(5777), 1179, doi:10.1126/science.1125566.

Gregory, J. M., et al. (2005), A model intercomparison of changes in the atlantic thermohaline circulation in response to increasing atmospheric CO_2 concentration, *Geophys. Res. Lett.*, *32*, L12703, doi:10.1029/2005GL023209.

Haine, T. W., et al. (2015), Arctic freshwater export: Status, mechanisms, and prospects, *Global Planet. Change*, *125*, 13–35, doi:10.1016/j.gloplacha.2014.11.013.

Held, I. M., and B. J. Soden (2006), Robust responses of the hydrological cycle to global warming, *J. Clim.*, *19*(21), 5686–5699, doi:10.1175/JCLI3990.1.

Hodson, D. L. R., S. P. E. Keeley, A. West, J. Ridley, E. Hawkins, and H. T. Hewitt (2013), Identifying uncertainties in Arctic climate change projections, *Clim. Dyn.*, *40*(11–12), 2849–2865, doi:10.1007/s00382-012-1512-z.

Holland, M. M., and C. M. Bitz (2003), Polar amplification of climate change in coupled models, *Clim. Dyn.*, *21*(3), 221–232, doi:10.1007/s00382-003-0332-6.

Holland, M. M., and L. Landrum (2015), Factors affecting projected Arctic surface shortwave heating and albedo change in coupled climate models, *Philos. Trans. R. Soc. A*, *373*(2045), 20140162, doi:10.1098/rsta.2014.0162.

Hu, Y., L. Tao, and J. Liu (2013), Poleward expansion of the Hadley circulation in CMIP5 simulations, *Adv. Atmos. Sci.*, *30*(3), 790–795, doi:10.1007/s00376-012-2187-4.

Hwang, Y. T., D. M. W. Frierson, and J. E. Kay (2011), Coupling between Arctic feedbacks and changes in poleward energy transport, *Geophys. Res. Lett.*, *38*, L17704, doi:10.1029/2011GL048546.

Johanson, C. M., and Q. Fu (2009), Hadley cell widening: Model simulations versus observations, *J. Clim.*, *22*(10), 2713–2725, doi:10.1175/2008JCLI2620.1.

Jungclaus, J. H., K. Lohmann, and D. Zanchettin (2014), Enhanced 20th-century heat transfer to the Arctic simulated in the context of climate variations over the last millennium, *Clim. Past*, *10*(6), 2201–2213, doi:10.5194/cpd-10-2895-2014.

Kay, J. E., M. M. Holland, C. M. Bitz, E. Blanchard-Wrigglesworth, A. Gettelman, A. Conley, and D. Bailey (2012), The influence of local feedbacks and northward heat transport on the equilibrium Arctic climate response to increased greenhouse gas forcing, *J. Clim.*, *25*(16), 5433–5450, doi:10.1175/JCLI-D-11-00622.1.

Koenigk, T., and L. Brodeau (2014), Ocean heat transport into the Arctic in the twentieth and twenty-first century in EC-Earth, *Clim. Dyn.*, *42*(11), 3101–3120, doi:10.1007/s00382-013-1821-x.

Laîné, A., M. Yoshimori, and A. Abe-Ouchi (2016), Surface Arctic amplification factors in CMIP5 models: Land and oceanic surfaces, seasonality, *J. Clim.*, *29*, 3297–3316, doi:10.1175/JCLI-D-15-0497.1.

Levitus, S., et al. (2012), World ocean heat content and thermosteric sea level change (0–2000 m), 1955–2010, *Geophys. Res. Lett.*, *39*, L10603, doi:10.1029/2012GL051106.

Lu, J., G. A. Vecchi, and T. Reichler (2007), Expansion of the Hadley cell under global warming, *Geophys. Res. Lett.*, *34*, L06805, doi:10.1029/2007GL030931.

Mahlstein, I., and R. Knutti (2011), Ocean heat transport as a cause for model uncertainty in projected Arctic warming, *J. Clim.*, *24*(5), 1451–1460, doi:10.1175/2010JCLI3713.1.

Manabe, S., and R. J. Stouffer (1980), Sensitivity of a global climate model to an increase of CO_2 concentration in the atmosphere, *J. Geophys. Res.*, *85*(C10), 5529–5554, doi:10.1029/JC085iC10p05529.

Marshall, J., K. C. Armour, J. R. Scott, Y. Kostov, U. Hausmann, D. Ferreira, T. G. Shepherd, and C. M. Bitz (2014), The ocean's role in polar climate change: Asymmetric Arctic and Antarctic responses to greenhouse gas and ozone forcing, *Philos. Trans. R. Soc. A*, *372*(2019), 20130040, doi:10.1098/rsta.2013.0040.

Marshall, J., J. R. Scott, K. C. Armour, J. M. Campin, M. Kelley, and A. Romanou (2015), The ocean's role in the transient response of climate to abrupt greenhouse gas forcing, *Clim. Dyn.*, *44*(7), 2287–2299, doi:10.1007/s00382-014-2308-0.

McCarthy, G. D., D. A. Smeed, W. E. Johns, E. Frajka-Williams, B. I. Moat, D. Rayner, M. O. Baringer, C. S. Meinen, J. Collins, and H. L. Bryden (2015), Measuring the Atlantic Meridional overturning circulation at 26°N, *Prog. Oceanogr.*, *130*, 91–111, doi:10.1016/j.pocean.2014.10.006.

Onarheim, I. H., T. Eldevik, M. Årthun, R. B. Ingvaldsen, and L. H. Smedsrud (2015), Skillful prediction of Barents Sea ice cover, *Geophys. Res. Lett.*, *42*, 5364–5371, doi:10.1002/2015GL064359.

Pithan, F., and T. Mauritsen (2014), Arctic amplification dominated by temperature feedbacks in contemporary climate models, *Nat. Geosci.*, *7*, 181–184, doi:10.1038/NGEO2071.

Rahmstorf, S., J. E. Box, G. Feulner, M. E. Mann, A. Robinson, S. Rutherford, and E. J. Schaaernicht (2015), Exceptional twentieth-century slowdown in Atlantic Ocean overturning circulation, *Nat. Clim. Change*, *5*, 475–480, doi:10.1038/nclimate2554.

Reintges, A., T. Martin, M. Latif, and N. S. Keenlyside (2016), Uncertainty in twenty-first century projections of the Atlantic Meridional Overturning Circulation in CMIP3 and CMIP5 models, *Clim. Dyn.*,1–17, doi:10.1007/s00382-016-3180-x.

Rugenstein, M. A. A., M. Winton, R. J. Stouffer, S. M. Griffies, and R. Hallberg (2013), Northern high-latitude heat budget decomposition and transient warming, *J. Clim.*, *26*(2), 609–621, doi:10.1175/JCLI-D-11-00695.1.

Saenko, O. A., J. C. Fyfe, and M. H. England (2005), On the response of the oceanic wind-driven circulation to atmospheric CO2 increase, *Clim. Dyn.*, *25*(4), 415–426, doi:10.1007/s00382-005-0032-5.

Spielhagen, R. F., K. Werner, S. A. Sørensen, K. Zamelczyk, E. Kandiano, G. Budeus, K. Husum, T. M. Marchitto, and M. Hald (2011), Enhanced modern heat transfer to the Arctic by warm Atlantic water, *Science*, *331*, 450–453, doi:10.1126/science.1197397.

Tandon, N. F., E. P. Gerber, A. H. Sobel, and L. M. Polvani (2013), Understanding Hadley cell expansion versus contraction: Insights from simplified models and implications for recent observations, *J. Clim.*, *26*(12), 4304–4321, doi:10.1175/JCLI-D-12-00598.1.

Tao, L., Y. Hu, and J. Liu (2016), Anthropogenic forcing on the Hadley circulation in CMIP5 simulations, *Clim. Dyn.*, *46*(9), 3337–3350, doi:10.1007/s00382-015-2772-1.

Trossman, D. S., J. B. Palter, T. M. Merlis, Y. Huang, and Y. Xia (2016), Large-scale ocean circulation-cloud interactions reduce the pace of transient climate change, *Geophys. Res. Lett.*, *43*, 3935–3943, doi:10.1002/2016GL067931.

Winton, M., S. M. Griffies, B. L. Samuels, J. L. Sarmiento, and T. L. Frölicher (2013), Connecting changing ocean circulation with changing climate, *J. Clim.*, *26*(7), 2268–2278, doi:10.1175/JCLI-D-12-00296.1.

Winton, M., W. G. Anderson, T. L. Delworth, S. M. Griffies, W. J. Hurlin, and A. Rosati (2014), Has coarse ocean resolution biased simulations of transient climate sensitivity', *Geophys. Res. Lett.*, *41*, 8522–8529, doi:10.1002/2014GL061523.

Wu, L., et al. (2012), Enhanced warming over the global subtropical western boundary currents, *Nat. Clim. Change*, *2*(3), 161–166, doi:10.1038/nclimate1353.

Yang, D., and O. A. Saenko (2012), Ocean heat transport and its projected change in CanESM2, *J. Clim.*, *25*(23), 8148–8163, doi:10.1175/JCLI-D-11-00715.1.

Yang, H., G. Lohmann, W. Wei, M. Dima, and J. Liu (2016), Intensification and poleward shift of subtropical western boundary currents under global warming, *J. Geophys. Res. Oceans*, *121*, 4928–4945, doi:10.1002/2015JC011513.

Yeager, S. G., A. R. Karspeck, and G. Danabasoglu (2015), Predicted slowdown in the rate of Atlantic sea ice loss, *Geophys. Res. Lett.*, *42*, 10,704–10,713, doi:10.1002/2015GL065364.

Zhang, R. (2015), Mechanisms for low-frequency variability of summer Arctic sea ice extent, *Proc. Natl. Acad. Sci. U.S.A.*, *112*(15), 4570–4575, doi:10.1073/pnas.1422296112.